Songho Kim
Raytheon UTD,
8350 Alban Road,
Springfield, VA 22150
e-mail: songho.kim@alumni.northwestern.edu

Carl Moore
Department of Mechanical Engineering,
Florida A&M University,
Tallahassee, FL 32310
e-mail: camoore@eng.fsu.edu

Michael Peshkin
e-mail: peshkin@northwestern.edu

J. Edward Colgate
e-mail: colgate@northwestern.edu

Department of Mechanical Engineering,
Northwestern University,
Evanston, IL 60208

Causes of Microslip in a Continuously Variable Transmission

The continuously variable transmission (CVT) is a type of transmission that can adopt any arbitrary gear ratio. Whereas typical transmissions utilize toothed gears, the CVT employs a sphere in rolling contact with a set of rollers; loads applied to the CVT are supported across these rolling contacts, resulting in microslips of varying amounts at each contact area. In this paper, we describe the causes of microslips in the CVT and ways to lessen them through an alternative CVT design. [DOI: 10.1115/1.2803711]

1 Introduction

Whereas typical transmissions that utilize combinations of gears can only adopt a fixed number of discrete transmission ratios, a continuously variable transmission, or simply CVT, can adopt any arbitrary gear ratio between a minimum and a maximum. There exist numerous CVT designs and applications: Engineers in the automotive industry, concerned with fuel efficiency, have developed CVTs for use in powertrains. In this application, the CVT ratio can be adjusted to match any engine speed to any vehicle speed. Hence with vehicles that employ CVTs, engineers are able to design controllers to maximize engine power to fuel consumption.

In the field of robotics, researchers at Northwestern University developed CVTs for use in human-machine devices, called cobots (short for collaborative robots) [1]. In the framework of a cobot, CVTs function as constraint mechanisms that place kinematic constraints on the cobot's joints.

1.1 Background. Most CVT only allow positive transmission ratios, but some can adopt both positive and negative transmission ratios; these latter transmissions are commonly known as infinitely variable transmissions, or simply IVTs.

The CVT, which is the focus of this paper, used in cobots is unique in that it can adopt any transmission ratio, including both positive and negative ∞. We may thus classify this particular transmission as an IVT; however, we will use the name and acronym given for this transmission in Ref. [2] and refer to it as the CVT.

CVTs are elemental in the design of a cobot. CVTs function as constraint mechanisms that are responsible for setting and enforcing the kinematic relationship of the cobot's joints. In the Arm cobot [3] for example, three CVTs set the kinematic relationship between the Arm's three rotational joints (Fig. 1). Servomotors, connected to each CVT, allow us to control the CVT settings in real time, thereby allowing us to control the Arm's end effector.

The design of the CVT utilizes a sphere that is surrounded and held in place by four rollers. Two of the four rollers, called steering rollers, constrain the sphere to rotate about an axis of rotation, whose direction can be changed by adjusting the orientations of the steering rollers. The relative velocities of the remaining two rollers, called drive rollers, are dependent on the orientation of the sphere's axis of rotation.

1.2 Motivation. The motivation for our analysis of the CVT stemmed from our physical interaction with existing cobots. We observed from our analysis of the cobots that the measured velocity ratios of a pair of joints, connected by CVTs, differed noticeably from the intended velocity ratios.

Ideally, the ratio of the angular velocities of a pair of robotic joints, connected by CVTs, is the same as the transmission ratios of the CVTs. In practice, however, the actual velocity ratio often deviates from the intended ratio. One contributor to this is microslip (or creep) across the rolling contacts between the CVT sphere and the rollers; a force on a robot's end point produces tractive forces across the rolling contacts, thereby giving rise to microslip (or creep) at these rolling contacts.

Herein, we develop a model of the CVT microslip, verify the model with experiments, and then use the model to simulate a proposed improvement to the CVT design.

1.3 Related Work. Akehurst et al. [4] give a good overview of published works related to CVTs that operate through rolling traction. Previous works concerning microslips in CVTs, utilized in cobots, are limited. They include the kinematic creep model [5] of Gillespie et al. and the experimental analysis [6] of Brokowski et al. of the CVT.

In Ref. [5], Gillespie et al. model the drive rollers as rigid bodies that make line contacts with the sphere. They describe that the drive rollers transmit longitudinal forces across the rolling contacts while under a state of spin.[1] In their work, Gillespie et al. determine an expression for the velocity ratio as a function of the transmission angle, load, and spin. The work of Gillespie et al. is limited to the analysis of slips at contacts between the sphere and the drive rollers; their work does not examine the causes and effects of slips at the contacts between the sphere and the steering

Contributed by the Power Transmission and Gearing Committee of ASME for publication in the JOURNAL OF MECHANICAL DESIGN. Manuscript received September 2, 2006; final manuscript received February 19, 2007; published online December 7, 2007. Review conducted by Teik C. Lim. Paper presented at the 2003 ASME International Mechanical Engineering Congress (IMECE2003), Washington, DC, November 15–21, 2003.

[1] Spin refers to relative angular motion of the normal of two bodies in contact.

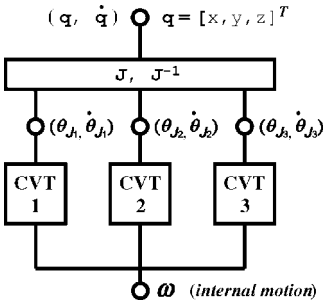

Fig. 1 Structure of the Arm cobot. The motions of the cobot's three rotational joints J_1, J_2, and J_3 are related to the cobot's internal motion as they are connected by three CVTs.

rollers.

The work of Brokowski et al. involves subjecting a physical CVT to experimental testing and comparing their results to the kinematic creep model of Gillespie et al. In their work, Browkowski et al. thoroughly examine the mechanics of the contacts between the sphere and the drive rollers, but like Gillespie et al., Browkowski et al. also neglect to examine causes and effects of slips of the contacts between the sphere and the steering rollers.

1.4 Preview of Sections. Our work concerns an experimental as well as an analytical analysis of the CVT. Through experimental analysis, we develop a kinetic model that describes the CVT's ability to produce the desired velocity ratios in the face of loads across the device. In addition, we develop an analytical model that describes the causes of microslips in the CVT and we offer suggestions for the design of an improved CVT.

In Sec. 2, we describe the design and kinematics of the CVT. In Sec. 3, we present an analytical model that describes the microslips in the CVT. In Sec. 4, we verify our model through experiments on a CVT that is subject to various loads. Finally, in Sec. 5, we describe the suggested designs of an improved CVT.

2 Continuously Variable Transmission

2.1 Continuously Variable Transmission Kinematics. The design of the CVT utilizes four rollers in rolling contact with a sphere (Fig. 2). Two of these rollers, called the *steering rollers*, constrain the sphere to rotate about a particular axis of rotation. The relative motions between the remaining two rollers, called the *drive rollers*, are dependent on the orientation of the sphere's axis of rotation.

In Fig. 3, the three-dimensional coordinate frame N, with coordinate axes x, y, and z, is fixed to the base of the CVT. The unit vectors $\mathbf{d}_1$, $\mathbf{d}_2$, and $\mathbf{d}_3$ are established by rotating the coordinate

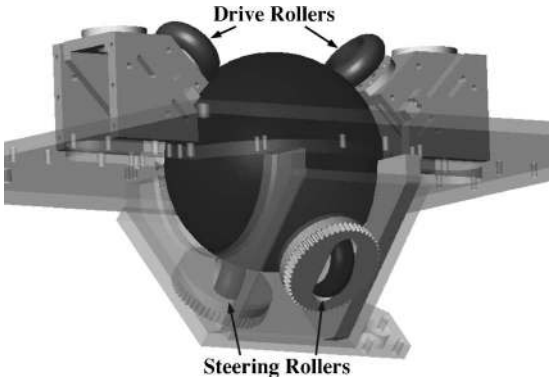

Fig. 2 A CAD model of the CVT. The design of the CVT employs a sphere in rolling contact with four rollers (two drive rollers and two steering rollers).

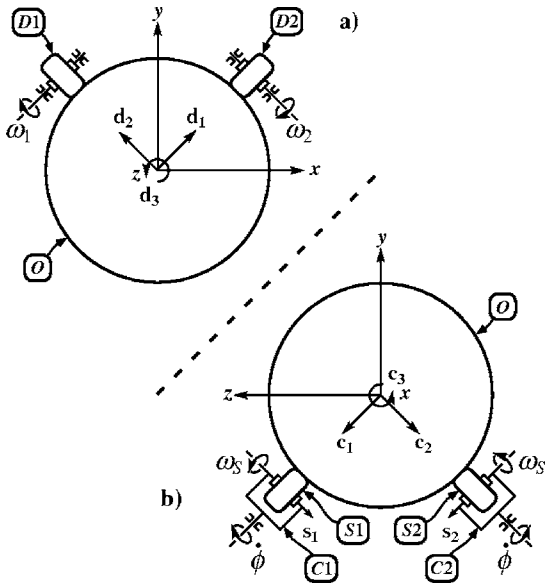

Fig. 3 The design of the CVT includes a sphere and four rollers. In (*a*), only the drive rollers are shown and in (b), only the steering rollers are shown.

frame N about the z-coordinate axis by 45 deg. The three orthogonal unit vectors $\mathbf{c}_i (i=1,2,3)$ are established by rotating the frame N about the x-coordinate axis by 135 deg. The unit vector $\mathbf{c}_3$ is in the positive x-coordinate direction. The unit vectors $\mathbf{c}_1$ and $\mathbf{c}_2$ are defined using the right-hand rule. The center of the sphere O is located at the origin of the coordinate frame N.

Figure 3(a) shows the drive Rollers $D1$ and $D2$. The center of the contact patch between the sphere O and the Roller $D1$ lies on an axis that is collinear to the unit vector $\mathbf{d}_2$. Drive Roller $D1$ has an angular velocity ω_1 about an axis that is parallel to the unit vector $\mathbf{d}_1$. The center of the contact patch between O and $D2$ lies on an axis that is collinear to the unit vector $\mathbf{d}_1$. Drive Roller $D2$ has an angular velocity ω_2 about an axis that is parallel to the vector $\mathbf{d}_2$.

Figure 3(b) shows the steering Rollers $S1$ and $S2$ and the steering Forks $C1$ and $C2$. $C1$ rotates about an axis that is collinear to the unit vector $\mathbf{c}_1$. The center of the contact patch between the sphere O and the Roller $S1$ lies on an axis that is collinear to the unit vector $\mathbf{c}_1$. $C2$ rotates about an axis that is collinear to the unit vector $\mathbf{c}_2$. The center of the contact patch between O and the Roller $S2$ lies on an axis that is collinear to the unit vector $\mathbf{c}_2$. $C1$ and $C2$ are mechanically coupled via a bevel gear (not shown) such that the orientations of $C1$ and $C2$ can be described by the same *steering angle* ϕ. The coordinate axis $\mathbf{s}_1$ is fixed to $C1$ and the coordinate axis $\mathbf{s}_2$ is fixed to $C2$. Steering Roller $S1$ has an angular velocity ω_S about $\mathbf{s}_1$ and steering Roller $S2$ has an angular velocity ω_S about $\mathbf{s}_2$.

Figure 4(a) shows the sphere O and steering Roller $S1$; steering Roller $S2$ and the two drive rollers are not shown. Figure 4(b) shows the sphere and the steering Roller $S2$; steering Roller $S1$ and the two drive rollers are not shown. Let r be the radius of the steering rollers and let R be the radius of the sphere O. Then, the rolling constraint between the Roller $S1$ and O, whose velocity is $\mathbf{\Omega}$, requires that

$$\mathbf{\Omega} \times R\mathbf{c}_1 = (\omega_S \cos\phi \mathbf{c}_2 + \omega_S \sin\phi \mathbf{c}_3) \times (-r\mathbf{c}_1) \tag{1}$$

Also, the rolling constraint between the Roller $S2$ and O requires that

$$\mathbf{\Omega} \times R\mathbf{c}_2 = (\omega_S \cos\phi \mathbf{c}_1 + \omega_S \sin\phi \mathbf{c}_3) \times (-r\mathbf{c}_2) \tag{2}$$

Combining Eqs. (1) and (2), we have

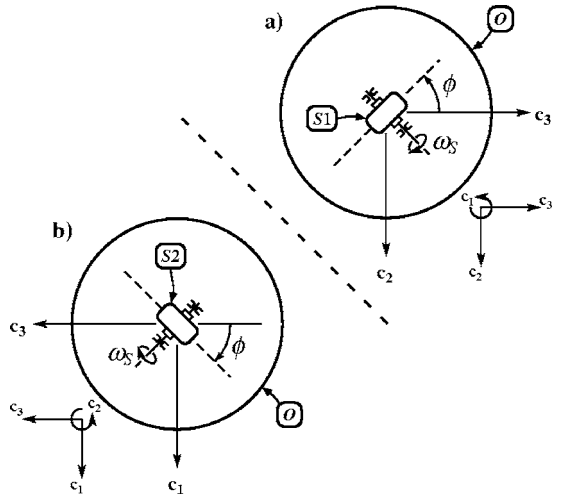

Fig. 4 Two additional views of the CVT. The orientations of both steering rollers are described by steering angle ϕ.

$$\boldsymbol{\Omega} = \frac{r\omega_S}{R}(-\cos\phi\mathbf{c}_1 - \cos\phi\mathbf{c}_2 - \sin\phi\mathbf{c}_3) \tag{3}$$

Or we may write

$$\boldsymbol{\Omega} = \frac{r\omega_S}{R}\left(\frac{\sqrt{2}\cos\phi - \sin\phi}{\sqrt{2}}\mathbf{d}_1 + \frac{\sqrt{2}\cos\phi + \sin\phi}{\sqrt{2}}\mathbf{d}_2\right) \tag{4}$$

We see that from the above equation, the sphere's instantaneous axis of rotation lies on a plane defined by the unit vectors $\mathbf{d}_1$ and $\mathbf{d}_2$.

Let t be an axis that is collinear to the sphere's instantaneous axis of rotation (Fig. 5) and let γ describe the angle between the unit vector $\mathbf{d}_1$ and the axis t. Then, γ, called the CVT angle, is related to the steering angle ϕ by

$$\gamma = \tan^{-1}\left(\frac{\sqrt{2} + \tan\phi}{\sqrt{2} - \tan\phi}\right) \tag{5}$$

Let ω_O be the sphere's angular velocity about the axis t. Then, the rolling constraint between the Roller $D1$ and the sphere O requires that

$$-\omega_1\mathbf{d}_1 \times -r\mathbf{d}_2 = (\omega_O\cos\gamma\mathbf{d}_1 + \omega_O\sin\gamma\mathbf{d}_2) \times R\mathbf{d}_2 \tag{6}$$

Also, the rolling constraint between the Roller $D2$ and the sphere O requires that

$$-\omega_2\mathbf{d}_2 \times -r\mathbf{d}_1 = (\omega_O\cos\gamma\mathbf{d}_1 + \omega_O\sin\gamma\mathbf{d}_2) \times R\mathbf{d}_1 \tag{7}$$

Equations (6) and (7) can be combined to find the relationship between the velocities of the drive rollers and the CVT angle γ:

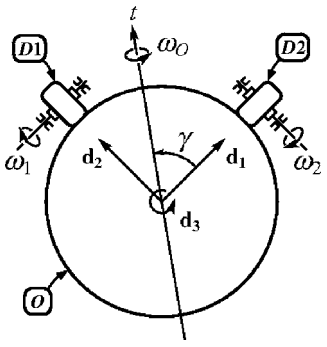

Fig. 5 The sphere's instantaneous axis of rotation is described by the CVT angle γ

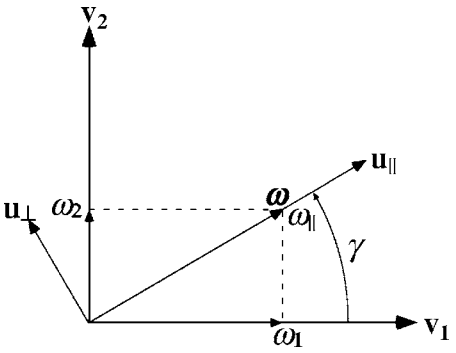

Fig. 6 Two-dimensional Cartesian coordinate system describing the velocities of the drive rollers

$$\frac{\omega_2}{\omega_1} = \tan\gamma \tag{8}$$

Equation (8) is called the *ideal transmission law*. We may combine Eqs. (5) and (8) to find an alternative expression of the ideal transmission law:

$$\frac{\omega_2}{\omega_1} = \frac{\sqrt{2} + \tan\phi}{\sqrt{2} - \tan\phi} \tag{9}$$

2.1.1 Continuously Variable Transmission Velocity Vector. We can express the velocities of both drive rollers as a vector in a two-dimensional Cartesian coordinate system (Fig. 6). The two-dimensional Cartesian coordinate system V has unit vectors $\mathbf{v}_1$ and $\mathbf{v}_2$ in the positive directions of the x- and y-coordinate axes, respectively. A point in the coordinate space V represents the displacements of drive Rollers $D1$ and $D2$; the x component represents the displacement of $D1$ and the y component represents the displacement of $D2$. A vector that locates this point represents the velocities of both drive rollers. The two-dimensional Cartesian coordinate system U is established by rotating coordinate system V about an axis that passes through coordinate system V's origin and normal to the $\mathbf{v}_1$-$\mathbf{v}_2$ plane by γ degrees. $\mathbf{u}_\parallel$ is called the *longitudinal velocity vector* and $\mathbf{u}_\perp$ is called the *lateral velocity vector*. $\mathbf{u}_\parallel$ is also called the *allowed direction of motion* and $\mathbf{u}_\perp$ is also called the *disallowed direction of motion*.

Let $\boldsymbol{\omega}$, called the CVT *velocity* vector, describe the velocities of both drive rollers. It may be expressed in the coordinate frame V:

$$\boldsymbol{\omega} = \omega_1\mathbf{v}_1 + \omega_2\mathbf{v}_2 \tag{10}$$

Or it may be expressed in the coordinate frame U:

$$\boldsymbol{\omega} = \omega_\parallel\mathbf{u}_\parallel + 0\mathbf{u}_\perp \tag{11}$$

where $\omega_\parallel$, called the CVT *parallel velocity*, describes the velocity of the CVT along its allowed direction of motion.

Given that frame U is rotated γ degrees from frame V, the velocities of the drive rollers may be written as

$$\omega_1 = \omega_\parallel\cos\gamma \tag{12}$$

$$\omega_2 = \omega_\parallel\sin\gamma \tag{13}$$

2.2 Continuously Variable Transmission Slip Angle. In practice, the ratio of the velocities between the two CVT drive rollers differs from that provided by the ideal transmission law (Eq. (8)). We describe this difference between the ratio given by Eq. (8) and the measured, or the actual, ratio of the velocities by an angle in the coordinate frame V.

We augment the two-dimensional Cartesian coordinate frame V with alpha (Fig. 7), called the CVT *slip angle*. Again, let the vector $\boldsymbol{\omega}$ describe the velocities of both drive rollers. In practice, $\boldsymbol{\omega}$ deviates from the longitudinal velocity vector $\mathbf{u}_\parallel$ such that it has

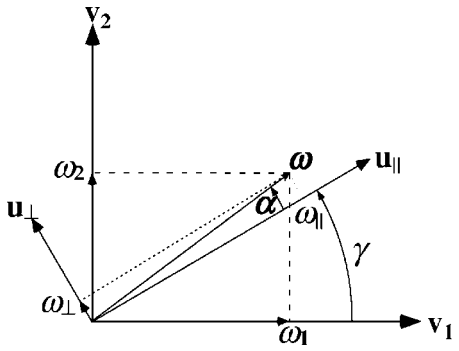

Fig. 7 Two-dimensional Cartesian coordinate system for the CVT with slip

components along both the allowed and disallowed ($\mathbf{u}_\perp$) directions of motion. Then, the velocity of the CVT is written as

$$\boldsymbol{\omega} = \omega_\parallel \mathbf{u}_\parallel + \omega_\perp \mathbf{u}_\perp \tag{14}$$

where $\omega_\perp$ is the vector component of the CVT's velocity vector along the disallowed direction of motion.

Let the angle γ_m describe the direction of the measured, or the actual, $\boldsymbol{\omega}$. Then, the difference between angles γ_m and γ yields the CVT slip angle (α):

$$\alpha = \gamma_m - \gamma \tag{15}$$

2.3 Torque Balance. Let τ_1 and τ_2 be the torques by the drive Rollers $D1$ and $D2$, respectively. Then, from Eq. (8), the torque balance equation for the CVT is

$$\frac{\tau_1}{\tau_2} = -\tan\gamma \tag{16}$$

2.3.1 Lateral and Parallel Torques. In practice, the pair of torques τ_1 and τ_2 often deviate from Eq. (16).

In Fig. 8, we express the pair of drive roller torques τ_1 and τ_2 as a single vector $\boldsymbol{\tau} = \tau_1 \mathbf{v}_1 + \tau_2 \mathbf{v}_2$ in the coordinate frame V, similar to that for $\boldsymbol{\omega}$ in Fig. 7.

Again, we augment coordinate frame V with coordinate frame U that is rotated about the origin by γ degrees. We can now express τ as a sum of the vector components along $\mathbf{u}_\parallel$ and $\mathbf{u}_\perp$:

$$\tau = \tau_\parallel \mathbf{u}_\parallel + \tau_\perp \mathbf{u}_\perp \tag{17}$$

The scalar component along $\mathbf{u}_\parallel$, $\tau_\parallel$, is called the *parallel torque* and the scalar component along $\mathbf{u}_\perp$, $\tau_\perp$, is called the *lateral torque*. Parallel torque $\tau_\parallel$ is the component of τ that is responsible for overcoming the CVT's internal friction and inertia and is also responsible for producing forward motion. Lateral torque $\tau_\perp$ is the component of τ that is supported internally by the CVT. $\tau_\perp$ is also known as CVT *load*; it is the load that is applied across the CVT.

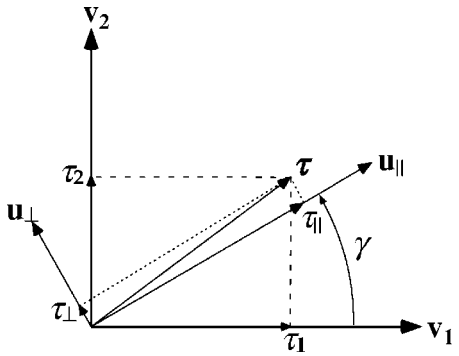

Fig. 8 The pair of drive roller torques τ_1 and τ_2 can be expressed as the sum of the lateral torque $\tau_\perp$ and the parallel torque $\tau_\parallel$

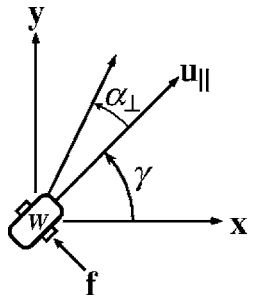

Fig. 9 Lateral slip angle $\alpha_\perp$

3 Modeled Slip Angles

Before we describe our CVT slip model, let us first describe two terms that we will use to develop our model.

3.1 Definitions. We will use the following two examples to describe *longitudinal slip ratio* and *lateral slip angle*.

3.1.1 Longitudinal Slip Ratio. A free-rolling wheel of radius r, whose translational velocity is v, has an angular velocity $\omega = v/r$. When the same wheel of radius r, whose translational velocity is again v, is called upon to transmit a tractive force against another body, the wheel incurs microslip at the interface between the two bodies in contact such that the angular velocity of the wheel differs from ω by $\Delta\omega$. In this example, the longitudinal slip ratio (ψ) is the ratio between ω by $\Delta\omega$:

$$\psi = \frac{\Delta\omega}{\omega} \tag{18}$$

3.1.2 Lateral Slip Angle. Figure 9 illustrates a plan view of wheel W in rolling contact with ground. The x-y coordinate frame is attached to ground. In the absence of an external forces, W rolls in the direction along the vector $\mathbf{u}_\parallel$, described by the orientation angle γ of W. When the same wheel is subjected to an external force perpendicular to $\mathbf{u}_\parallel$, the wheel rolls in the direction of a vector described by γ plus lateral slip angle $\alpha_\perp$.

3.2 Modeled Steering Roller Slip Angle. The steering rollers constrain the CVT sphere to rotate about a particular axis of rotation.

A load across the CVT ($\tau_\perp$) is supported internally within the CVT across four contacts between the sphere and the steering and drive rollers. The two drive rollers support tractive forces in the direction of rolling, and the two steering rollers support forces lateral to the direction of rolling (Fig. 10).[2]

Let $\mathbf{f}_\perp^{S1}$ be the lateral force imparted on the Roller $S1$ by the sphere O. Then, from Ref. [7], we know that $\mathbf{f}_\perp^{S1}$ is a function of $\tau_\perp$ and ϕ:

$$\mathbf{f}_\perp^{S1} = \frac{\tau_\perp \cos\gamma}{r\sqrt{2}\cos\phi - \sin\phi}[0\mathbf{c}_1 - \cos\phi\mathbf{c}_2 - \sin\phi\mathbf{c}_3]^T \tag{19}$$

where r is the radius of the steering rollers and γ is the transmission angle. To simplify the above algebraic expression, both γ and ϕ are used. Recall that γ and ϕ are related as described in Eq. (5).

Let $\mathbf{f}_\perp^{S2}$ be the lateral force imparted on the Roller $S2$ by the sphere O. Then,

$$\mathbf{f}_\perp^{S2} = \frac{\tau_\perp \cos\gamma}{r\sqrt{2}\cos\phi - \sin\phi}[\cos\phi\mathbf{c}_1 0\mathbf{c}_2 \sin\phi\mathbf{c}_3]^T \tag{20}$$

[2]A summary of the internal forces within the CVT can be found in Ref. [7].

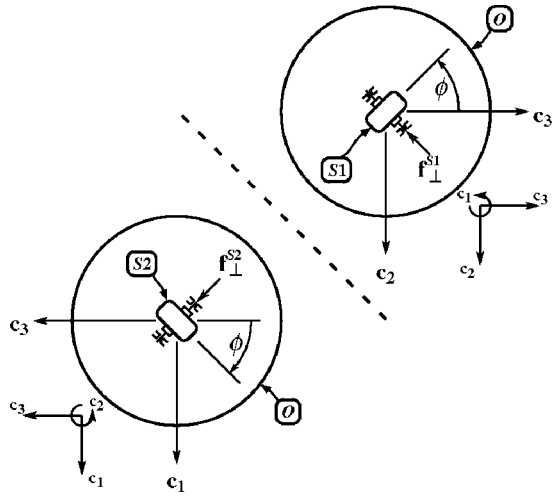

Fig. 10 Lateral forces are imparted on the steering rollers by the sphere

Let $\alpha_\perp^{S1}$ be the lateral slip angle by the Roller $S1$ and let $\alpha_\perp^{S2}$ be the lateral slip angle by the Roller $S2$. Let us model the angles $\alpha_\perp^{S1}$ and $\alpha_\perp^{S2}$ to be directly related to the lateral forces that they support:

$$\alpha_\perp^{S1} = \varepsilon_S \frac{\tau_\perp \cos\gamma}{r\sqrt{2}\cos\phi - \sin\phi} \cdot \left[\begin{bmatrix} 0\mathbf{c}_1 \\ -\omega_S \sin\phi\mathbf{c}_2 \\ \omega_S \cos\phi\mathbf{c}_3 \end{bmatrix} \times \begin{bmatrix} 0\mathbf{c}_1 \\ -\cos\phi\mathbf{c}_2 \\ -\sin\phi\mathbf{c}_3 \end{bmatrix} \right] \cdot \mathbf{c}_1 \tag{21}$$

$$\alpha_\perp^{S2} = \varepsilon_S \frac{\tau_\perp \cos\gamma}{r\sqrt{2}\cos\phi - \sin\phi} \cdot \left[\begin{bmatrix} \omega_S \sin\phi\mathbf{c}_1 \\ 0\mathbf{c}_2 \\ -\omega_S \cos\phi\mathbf{c}_3 \end{bmatrix} \times \begin{bmatrix} \cos\phi\mathbf{c}_1 \\ 0\mathbf{c}_2 \\ \sin\phi\mathbf{c}_3 \end{bmatrix} \right] \cdot -\mathbf{c}_2 \tag{22}$$

where ε_S, called the *lateral slip constant*, has the unit 1/N. Its value is dependent on the geometry of the contact patch, material properties of the roller and the sphere, normal force, etc., $\mathbf{c}_1$ and $-\mathbf{c}_2$ ensure correct signs.

After some algebra, it can be shown that $\alpha_\perp^{S1} = \alpha_\perp^{S2}$. Therefore, let $\alpha_\perp = \alpha_\perp^{S1} = \alpha_\perp^{S2}$. Let the angle γ_a describe the sphere's actual axis of rotation. Whereas angle γ describes the *expected* axis of rotation associated with the steering angle ϕ, γ_a describes the sphere's *actual* axis of rotation. After some algebra, we can show γ_a to be a function of ϕ and $\alpha_\perp$:

$$\gamma_a = \tan^{-1}\left(\frac{\sqrt{2} + \tan(\phi + \alpha_\perp)}{\sqrt{2} - \tan(\phi + \alpha_\perp)} \right) \tag{23}$$

Then, the *modeled* steering roller slip angle α_{SR} is simply the difference between γ_a and γ:

$$\alpha_{SR} = \gamma - \gamma_a \tag{24}$$

3.3 Modeled Drive Roller Slip Angle. In the case of an ideal CVT, the velocity of drive Roller $D1$, ω_1, is related to the parallel velocity $\omega_\parallel$ and transmission angle γ: $\omega_1 = \omega_\parallel \cos\gamma$ (Eq. (13)). In practice, however, $\omega_1 \neq \omega_\parallel \cos\gamma$.

Let ψ_1 be the longitudinal slip ratio of Roller $D1$. Due to microslip incurred by $D1$, ω_1 differs from $\omega_\parallel \cos\gamma$ by $\Delta\omega_1$. Then, from Eq. (18),

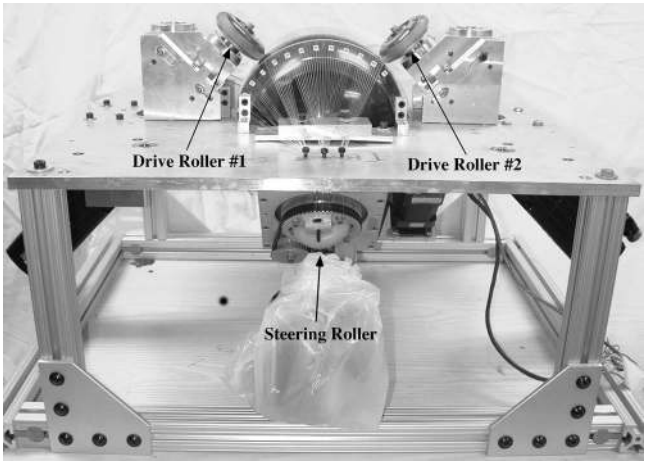

Fig. 11 The physical CVT used for experimental testing

$$\psi_1 = \frac{\Delta\omega_1}{\omega_\parallel \cos\gamma} \tag{25}$$

Similarly, for drive Roller $D2$, ω_2 differs from $\omega_\parallel \sin\gamma$ by $\Delta\omega_2$. Again, from Eq. (18),

$$\psi_2 = \frac{\Delta\omega_2}{\omega_\parallel \sin\gamma} \tag{26}$$

Given a load $\tau_\perp$ and a transmission angle γ, Roller $D1$ transmits a tractive force $-\tau_\perp \sin\gamma / r$ on the surface of the sphere, where r is the radius of the drive rollers. Similarly, $D2$ transmits a tractive force $\tau_\perp \cos\gamma / r$ on the surface of the sphere.

Let us model the ratios ψ_1 and ψ_2 to be linearly related to the tractive forces that the drive rollers transmit:

$$\psi_1 = \varepsilon_D \left| \frac{\tau_\perp \sin\gamma}{r} \right| \mathrm{sgn}(-\omega_\parallel \tau_\perp \sin\gamma\cos\gamma) \tag{27}$$

and

$$\psi_2 = \varepsilon_D \left| \frac{\tau_\perp \cos\gamma}{r} \right| \mathrm{sgn}(\omega_\parallel \tau_\perp \sin\gamma\cos\gamma) \tag{28}$$

where ε_D, called the *longitudinal slip constant*, has the unit 1/N. The terms $\mathrm{sgn}(-\omega_\parallel \tau_\perp \sin\gamma\cos\gamma)$ and $\mathrm{sgn}(\omega_\parallel \tau_\perp \sin\gamma\cos\gamma)$ ensure correct signs.

Incorporating longitudinal slips of both drive rollers, we have

$$\omega_1 = \omega_\parallel \cos\gamma(1 + \psi_1) \tag{29}$$

$$\omega_2 = \omega_\parallel \sin\gamma(1 + \psi_2) \tag{30}$$

The actual velocities of the drive rollers, ω_1 and ω_2, may be expressed as a vector in V space (Eq. (10)); let the angle γ_m describe the direction of this vector. Then, *drive roller slip angle* α_{DR} can be found by subtracting γ_a from γ_m:

$$\alpha_{DR} = \gamma_m - \gamma_a \tag{31}$$

3.4 Modeled Slip Angle. The modeled drive roller slip angle and the steering roller slip angle are summed to find the modeled CVT slip angle α:

$$\alpha = \alpha_{SR} + \alpha_{DR} \tag{32}$$

4 Experimental Analysis

In this chapter, we describe the setup and experimental analysis of a CVT that is subject to various loads.

4.1 Experimental Setup. Figure 11 shows the actual CVT used for experimental testing. The two drive rollers are labeled.

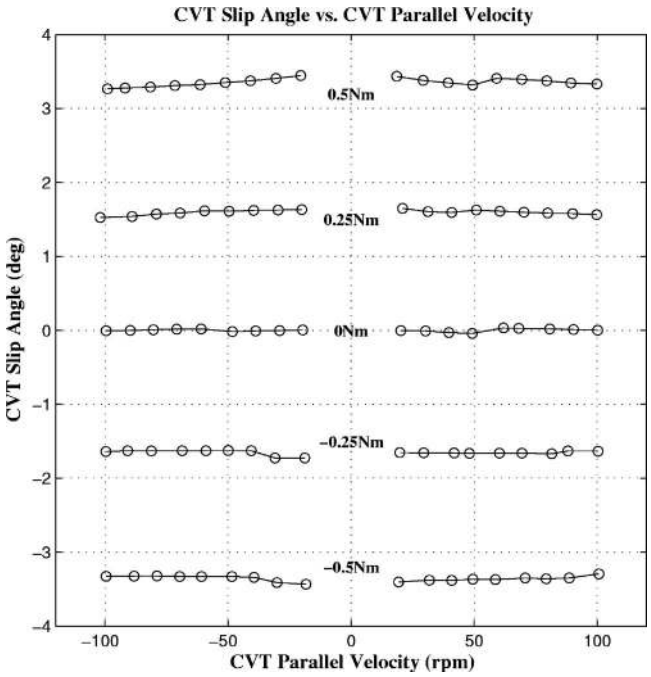

Fig. 12 CVT slip angle α versus CVT parallel velocity $\omega_{\|}$ at various CVT loads

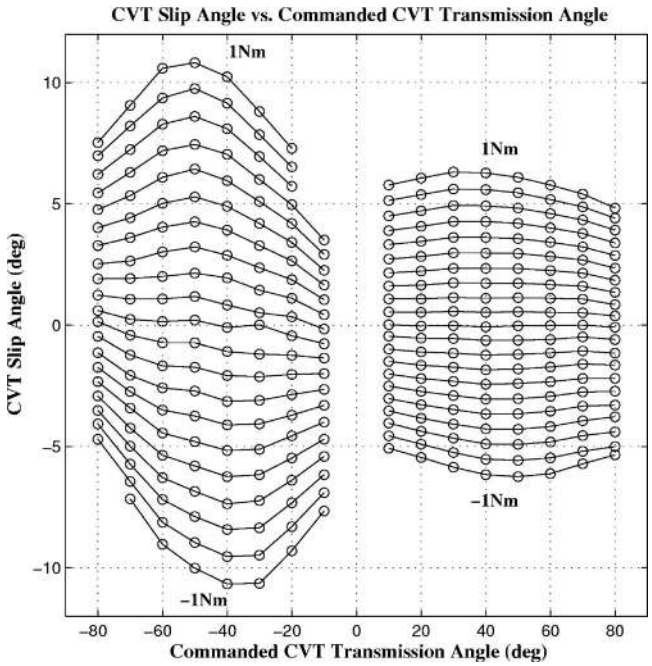

Fig. 13 Measured α. CVT loads are between −1 Nm and 1 Nm in 0.1 Nm increments.

Only one of the two steering rollers is visible. A servomotor, used to generate CVT load, is directly coupled to each of the two drive rollers. The drive rollers are 82a durometer in-line skating wheels; they are 80 mm in diameter. The steering rollers are 84a durometer in-line skating wheels; they are 76 mm in diameter.

4.2 Testing Protocol. We are interested in finding the correlation between the CVT slip angle (α), velocity (ω), transmission angle (γ), and load ($\tau_{\perp}$). In our experiments, the transmission angles are set to values between −80 deg and +80 deg at 10 deg increments, and the CVT loads are set to values between −1.0 Nm and 1.0 Nm at 0.1 Nm increments.

The CVT load is considered to be positive if the following is true:

$$|(\omega_1 \mathbf{v}_1 + \omega_2 \mathbf{v}_2) \times (\tau_1 \mathbf{v}_1 + \tau_2 \mathbf{v}_2)| > 0 \tag{33}$$

and negative if the following is true:

$$|(\omega_1 \mathbf{v}_1 + \omega_2 \mathbf{v}_2) \times (\tau_1 \mathbf{v}_1 + \tau_2 \mathbf{v}_2)| < 0 \tag{34}$$

4.3 Experimental Results. With the first set of experiments, we want to determine if there exists a correlation between the CVT slip angle and the CVT velocity.

In Fig. 12, we show the measured CVT slip angles (y axis) versus the CVT velocity (x axis) at various CVT loads with the transmission angle set to 45 deg. Figure 12 shows a lack of correlation between the CVT slip angle and CVT velocity[3] and thus we may reasonably conclude that the measure of the slip angles is independent of the CVT velocity ω. We may, therefore, carry out our experimental analysis of the CVT at any CVT velocity.

4.3.1 Measured Slip Angle. The measured velocities of both drive rollers may be expressed as vector ω in the coordinate frame Σ (Fig. 7). Let the angle γ_m describe the direction of this vector (Fig. 7). Then, the CVT slip angle α is the difference between the angle γ_m and the CVT angle γ:

$$\alpha = \gamma_m - \gamma \tag{35}$$

Figure 13 shows the measured CVT slip angle versus the CVT angle at CVT loads from −1 Nm to 1 Nm in 0.1 Nm increments.

4.3.2 Measured Steering Roller Slip Angle. The measured steering roller slip angle α_{SR} can be found by measuring the difference between the measured axis of rotation angle and the commanded axis of rotation angle (also called the CVT angle) (Eq. (24)). We were able to determine the actual axis of rotational angle visually, using a grid of closely spaced wires placed a few millimeters above the sphere. Figure 14 shows the measured steer-

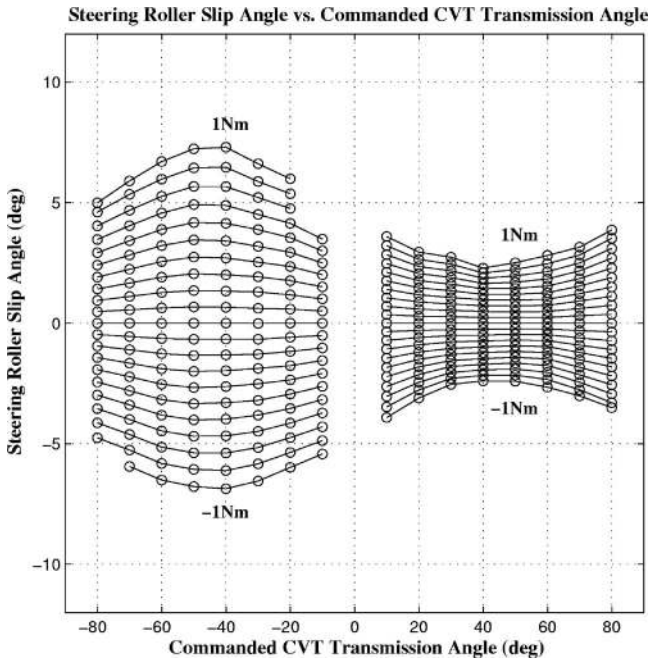

Fig. 14 Measured α_{SR}

[3]Experimental results for other transmission angles also yield little correlation between α and CVT velocity.

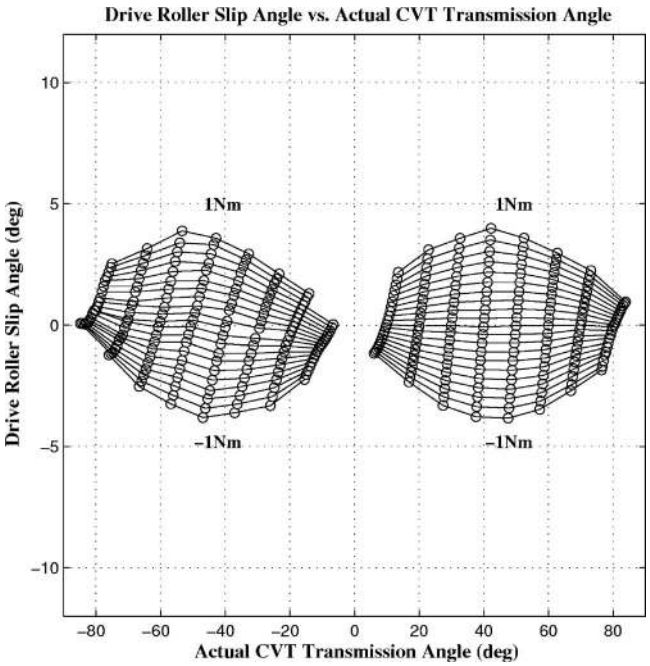

Fig. 15 Measured α_{DR}. The drive roller slip angles are plotted against the sphere's actual transmission angle.

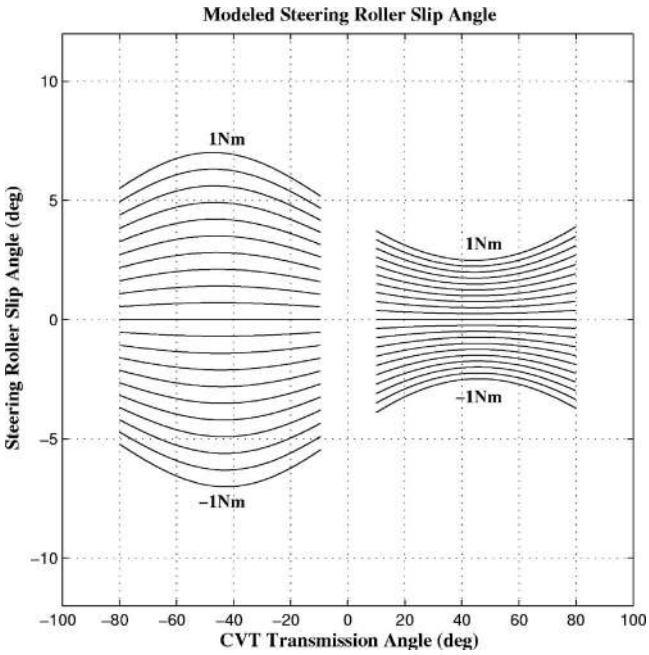

Fig. 16 Modeled α_{SR}. ε_S=0.0049 N^{-1}.

ing roller slip angle α_{SR} versus the commanded CVT angle γ at various CVT loads $\tau_\perp$.

4.3.3 Measured Drive Roller Slip Angle. We can find the measured drive roller slip angle α_{DR} using Eq. (31). Figure 15 shows the measured drive roller slip angle α_{DR}.

Note that we have plotted the drive roller slip angles versus the *actual* transmission angles (γ_a) rather than the CVT angles (γ), thereby isolated the measurements of the physical effects at the rolling contacts between the sphere and the drive rollers.

4.4 Comparison Between Measured and Modeled Slips. Now that we found the slips experimentally, we can compare it to our slip models. Recall that our models have just two constants, ε_S and ε_D, for us to define. First, we adjust ε_S so that our modeled steering roller slip angles closely match the measured steering roller slip angles. A comparison between Figs. 16 and 14 shows that our model accurately describes the physical effects at the contacts between the steering rollers and the CVT sphere. Next, we adjust ε_D so that the modeled drive roller slip angles closely match the measured drive roller slip angles. A comparison between Figs. 17 and 15 shows that our drive roller slip model closely describes the physical effects at the contacts between the drive rollers and the CVT sphere.

Finally, we sum the modeled slip angles α_{DR} and α_{SR} to find the modeled CVT slip angle α. A comparison between Figs. 18 and 13 shows that our CVT slip model closely describes the various slips that take place at all four rolling contacts between the sphere and the rollers.

5 Suggested Design of the Continuously Variable Transmission

5.1 Placement and Number of Rollers. Having determined the values of the constants ε_D and ε_S, we can predict the slip angles of a CVT with a different roller configuration. Consider the *box* CVT that is discussed in Ref. [1].

The differences between the box CVT and the existing CVT are in the placements of the steering rollers and the addition of follower rollers.

The number and the arrangement of the drive rollers in the box CVT lessen the amount of slipover, which is incurred in the existing CVT. In the box CVT, the drive rollers (A and B in Fig. 19) are mechanically coupled to follower rollers (A′ and B′ in Fig. 19). Whereas in the existing CVT, tractive forces by the drive rollers were supported by just two drive rollers, tractive forces in the box CVT are supported by four drive rollers, thereby essentially halving the drive roller slip angle.

Another difference between the two CVTs is that the box CVT employs additional steering rollers that are positioned at different positions around the sphere. This setup significantly lessens the amount of slip incurred by the steering rollers as we will show later.

Figure 19 shows the suggested design of the CVT. The pro-

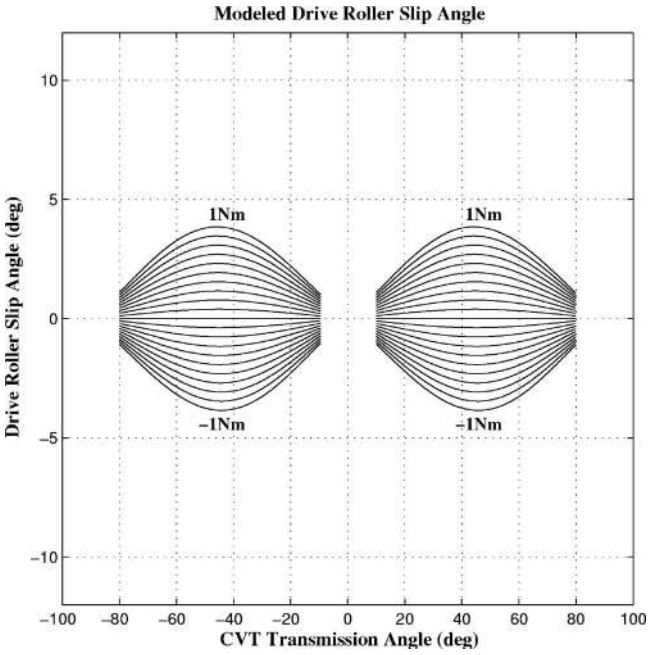

Fig. 17 Modeled α_{DR}. ε_D=0.0038 N^{-1}.

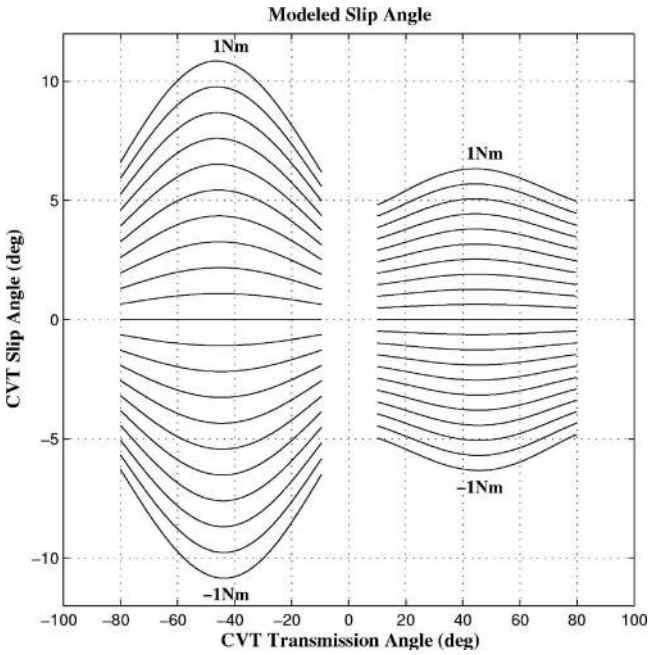

Fig. 18 Modeled α. ε_S=0.0049 N^{-1}, ε_D=0.0038 N^{-1}.

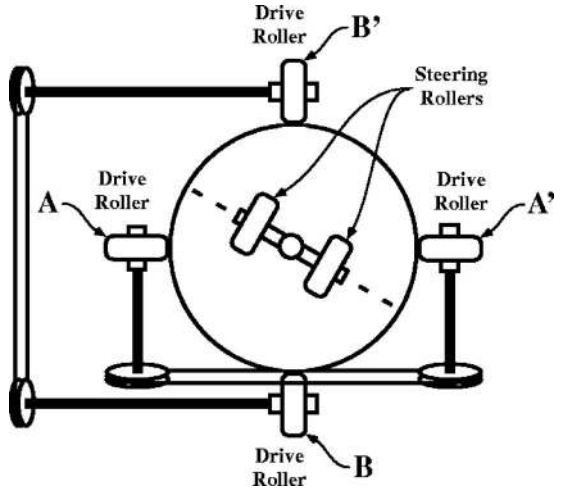

Fig. 19 Suggested design of the box CVT

posed CVT employs a pair of Rollers A and A′ that are mechanically coupled. These two rollers transmit motions and torques to a single rotational joint of a mechanical system, such as a robot. Rollers B and B′ are also mechanically coupled; they both transmit motions and torques to a second rotational joint. Two sets of a pair of steering rollers (each separated by a distance d) are located on opposite ends of the sphere.

Let us assume that the box CVT employs the same types of rollers and sphere as the existing CVT. Let us also assume that the preload force is the same as it was for our experiment. We can then predict the slip angles α, α_{SR}, and α_{DR} for the box CVT (with ε_D=0.0038 N^{-1} and ε_S=0.0049 N^{-1}).

Figure 20 shows the steering roller slip angles and the drive roller slip angles for the existing CVT (Fig. 2) and Fig. 21 shows the slip angles for the box CVT. A comparison between Figs. 20 and 21 shows that slip angles are smaller in the box CVT than in the existing CVT.

The existing CVT employs two steering rollers to constrain the sphere to rotate about a particular axis of rotation, whereas the box CVT employs four steering rollers to accomplish the same task. A load across the CVT creates a moment about an axis that must be balanced by the tractive forces at the rolling contacts between the sphere and the steering rollers. Since the box CVT employs more steering rollers than the existing CVT, they are required to support lesser tractive forces.

One other improvement over the existing CVT is the position of the steering rollers about the surface of the sphere. In the box CVT, the steering rollers are positioned about the sphere such that their tractive forces produce the maximal moment about the sphere.

6 Conclusion

In this paper, we presented experimental results that showed that loads across the CVT cause the velocities of the CVT joints to differ from the intended velocities. Our experimental results showed that for a particular transmission angle, the difference between the actual velocity ratio and the ideal velocity ratio is linearly related to the load applied across the CVT. We observed that the cause of this difference is microslip at the rolling contacts between the sphere and the rollers. The CVT's steering rollers incurred lateral slip, resulting in the sphere's axis of rotation deviating from the intended tilt angle. The CVT's drive rollers incurred longitudinal slip due to tractive forces that they had to support.

The lateral and longitudinal slips incurred by the steering and drive rollers were characterized by two constants ε_D and ε_S, each

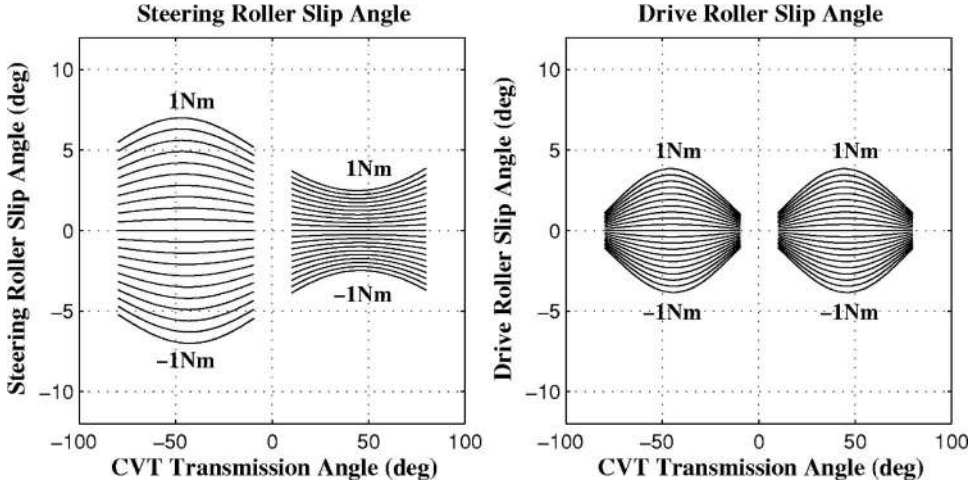

Fig. 20 Slip angles for the existing CVT

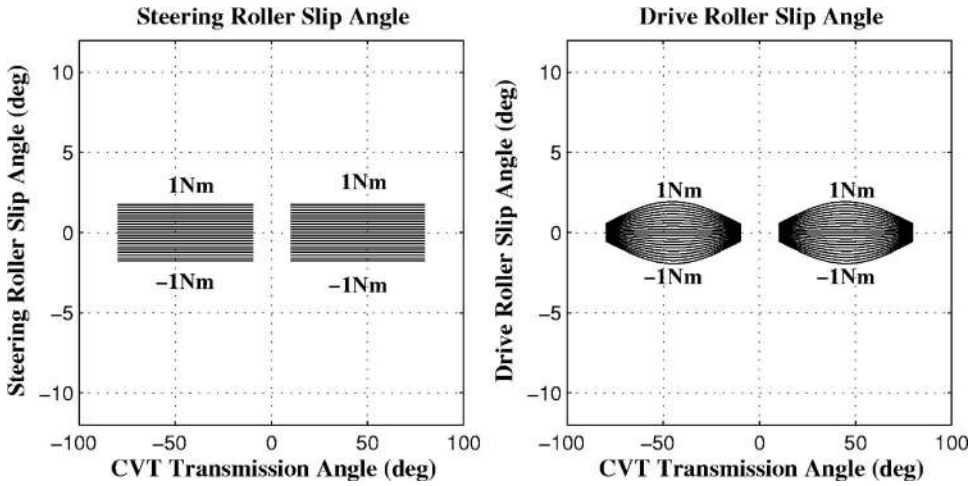

Fig. 21 Slip angles for the box CVT

relating the measures of the slips to the tractive forces supported across the rolling contacts. After having found the values of these two constants, we showed that the proposed *box* CVT would perform superior to the existing CVT.

References

[1] Peshkin, M. A., Colgate, J. E., Wannasuphoprasit, W., Moore, C. A., and Gillespie, R. B., 2001, "Cobot Architecture," IEEE Trans. Rob. Autom., **17**(4), pp. 377–390.

[2] Moore, C. A., 1997, "Continuously Variable Transmission for Serial Link Cobot Architecture," MS thesis, Northwestern University, Evanston, IL.

[3] Moore, C. A., Peshkin, M. A., and Colgate, J. E., 2003, "Cobot Implementation of Virtual Paths and 3D Virtual Surfaces," IEEE Trans. Rob. Autom., **19**(2), pp. 347–351.

[4] Akehurst, S., Parker, D. A., and Schaaf, S., 2006, "CVT Rolling Traction Drives—A Review of Research Into Their Design, Functionality, and Modeling," ASME J. Mech. Des., **128**(5), pp. 1165–1176.

[5] Gillespie, R. B., Moore, C. A., Peshkin, M. A., and Colgate, J. E., 2002, "Kinematic Creep in a Continuously Variable Transmission: Traction Drive Mechanics for Cobots," ASME J. Mech. Des., **124**(4), pp. 713–722.

[6] Brokowski, M., Kim, S., Colgate, J. E., Gillespie, R., and Peshkin, M., 2002, "Toward Improved CVTs: Theoretical and Experimental Results," *ASME International Mechanical Engineering Congress and Exposition*, New Orleans, LA.

[7] Kim, S., 2003, "Control of the Powered Armcobot and Analysis of a Continuously Variable Transmission," Ph.D. thesis, Northwestern University, Evanston, IL.